Individualized Structure–Function Mapping for Glaucoma: Practical Constraints on Map Resolution for Clinical and Research Applications

Jonathan Denniss,[1,2] Andrew Turpin,[2] and Allison M. McKendrick[1]

[1]Department of Optometry and Vision Sciences, The University of Melbourne, Australia
[2]Department of Computing and Information Systems, The University of Melbourne, Australia

Correspondence: Allison M. McKendrick, Department of Optometry and Vision Sciences, Level 4 Alice Hoy Building, The University of Melbourne, Parkville, VIC 3010, Australia; allisonm@unimelb.edu.au.

Submitted: December 11, 2013
Accepted: February 12, 2014

Citation: Denniss J, Turpin A, McKendrick AM. Individualized structure–function mapping for glaucoma: practical constraints on map resolution for clinical and research applications. *Invest Ophthalmol Vis Sci.* 2014;55:1985–1993. DOI:10.1167/iovs.13-13758

Purpose. We have developed customized maps that relate visual field and optic nerve head (ONH) regions according to individual anatomy. In this study, we aimed to determine feasible map resolution for research use, and to make a principled recommendation of sector size for clinical applications.

Methods. Measurement variability in fovea–ONH distance and angle was estimated from 10 repeat OCT scans of 10 healthy people. Errors in estimating axial length from refractive error were determined from published data. Structure–function maps were generated, and customized to varied clinically-plausible anatomical parameters. For each parameter set (n = 210), 200 maps were generated by sampling from measurement/estimation error distributions. Mapped 1° sectors at each visual field location from each parameter set were normalized to difference from their mean. Variation (90% ranges) in normalized mapped sectors represents the precision of individualized maps.

Results. Standard deviations of repeated measures of fovea–ONH distance and angle were 61 μm and 0.97° (coefficients of variation 1.3% and 12.0%, respectively). Neither measure varied systematically with mean (Spearmans's $\rho = 0.26$, $P = 0.47$ for distance, $\rho = -0.31$, $P = 0.39$ for angle). Variation (90% ranges) in normalized mapped sectors varied across the visual field and ranged from 3° to 18° when axial length was measured accurately, and from 6° to 32° when axial length was estimated from refractive error.

Conclusions. The 90% ranges represent the minimum feasible ONH sector size at each visual field location. For clinical use an easily interpretable scheme of 30° sectors is suggested.

Keywords: structure–function, visual field, optic nerve head, glaucoma, perimetry

In glaucoma and other optic neuropathies no single test can currently provide a complete picture of a patient's disease state. It is common in clinical practice to combine information from several tests in order to increase certainty in diagnosis of disease or disease progression. Combining information from localized measurements of ocular structure, such as retinal nerve fiber layer (RNFL) thickness, and visual function, such as visual field sensitivity, requires the use of a structure–function map that relates regions of the visual field to areas of the relevant ocular structure. Population average maps[1–4] have become established in clinical and research use for this purpose; however, recent studies have highlighted considerable between-individual variability in the mapping of visual field regions to the optic nerve head (ONH).[5,6] It is possible that by producing structure–function maps that are customized to the individual patient, better concordance between measurements may be obtained, improving the information available to the clinician.

In previous articles,[7,8] we have described a computational model that maps any given retinal location to the ONH, customized to the individual patient's ocular anatomy. We have also shown that the major influences on the mapping of the 24-2 visual field locations typically tested in clinical practice to the ONH are the position of the ONH relative to the fovea and axial length.[8] The maps produced by the model broadly agree with the established population-average maps,[8] and the influences of ocular anatomical variation have proved strikingly similar to the results of a recent empirical study of visible nerve fiber bundle pathways in retinal images.[6] Further, we have demonstrated agreement between the mapping predicted by the model and maps produced by hand-tracing of visible nerve fiber bundle pathways in individual retinal images.[9]

The model takes measurements of axial length and ONH position as inputs, and maps the given set of visual field locations to the ONH in 1° sectors. In clinical practice, measurements of ONH position relative to the fovea can be made by imaging instruments such as optical coherence tomographers, while axial length measurements can be obtained by biometry, or estimated from refractive error.[10–13] These measurements, however, are associated with a degree of error that affects the precision with which we can map individualized structure and function. This effect is borne out clinically as a widening of the necessary size of ONH sectors used in structure–function mapping, such that where anatomical measurements are imprecise, sector size must be increased. The effect of anatomical measurement imprecision on mapping individual visual field locations to the ONH is, however, unlikely to be uniform across the visual field, due to the

nonuniform effect of anatomical variation on mapping of individual locations.[8]

In this study, we investigate the effects of imprecision in clinical measurement of ONH position and axial length on the mapping of visual field locations to the ONH using our previously described model.[7,8] We use this information to derive a principled, overall sector size that can be used for general clinical application of individualized structure–function mapping, as well as identifying local variations in a minimum feasible sector size that may be useful for research applications. We further demonstrate the clinical application of individualized structure–function mapping using the derived sectors by means of case examples. Ultimately, we aim to facilitate the transition of individualized structure–function mapping from the laboratory to general clinical use in glaucoma and other optic neuropathies.

Methods

ONH Position

The position of the ONH relative to the fovea, measured by distance and angle, can be captured clinically using readily available imaging devices. In this study, we used an optical coherence tomographer (Spectralis; Heidelberg Engineering GmbH, Heidelberg, Germany). Following RNFL circle scans, the instrument provides the angle (degrees) between the fixation point and the center of the user-placed scan circle around the ONH, relative to horizontal. The distance (μm) between these two locations can then be measured using the caliper tool in the instrument software provided.

To determine the precision of fovea–ONH distance and angle measurements made this way, we studied one eye each of 10 healthy, young adults who were imaged with the RNFL circle scan protocol of the optical coherence tomographer 10 times in a single session. Participants were aged 23 to 43 years, had Snellen visual acuity 6/6 or better with spectacle correction, refractive error less than 5.00 diopters (D) spherical equivalent and 1.50 D cylinder, clear ocular media, and no current or previous ocular disease. In between image captures, the participants moved away from the instrument and the instrument was repositioned into a random position in order to simulate the clinical scenario, whereby patients are imaged once only. There are three main sources of variation in these measurements: variations in the positioning of the scan circle by the operator, variations in head position by the subject, and variations in fixation that affect the accuracy of the registration with the fovea. The same experienced operator captured all the images, and took care to center the scan circle on the ONH as accurately as possible. The operator also monitored image quality, ensuring that the captured fundus image was well focused and evenly illuminated, and the optical coherence tomography (OCT) image quality was greater than 20 dB. Any poor images were recaptured. Subjects were asked to position their head straight on the chin/forehead rest as would be done in clinic, and no further adjustment was made. Registration of previous images was not used. Fixation variation was minimized by recapturing images where there was a clear misregistration between the fixation location and the fovea in the infrared retinal image. Within-subject variability in fovea–ONH distance and angle measurements was assessed for use as input to the structure–function model (see the Structure–Function Mapping Simulations section). Ethics approval for collection of these data was given by the University of Melbourne Human Research ethics committee (Melbourne, Australia). The study protocol adhered to the tenets of the Declaration of Helsinki, and all subjects provided written informed consent to participate.

Estimation of Axial Length From Refractive Error

Since axial length and spherical equivalent refractive error are linearly related in phakic eyes,[10–13] it is possible to estimate axial length from refractive error. In clinical scenarios where axial length is not routinely measured (such as in the management of glaucoma), estimating the axial length input to the structure–function model from available information that does not require the use of an additional instrument may be beneficial. For this reason, we investigated the error in estimating axial length from refractive error, based on the findings of previous studies.[12,13]

Axial length and spherical equivalent refractive error data from myopic eyes ($n = 87$, refractive error range, −11.95–0.74 D) were digitized from Figure 3A of Atchison et al.[12] Similar data for hypermetropic eyes ($n = 43$, refractive error range, 1.08–9.35 D) were digitized from Figure 3 of Mallen et al.[13] It was not possible to digitize all the data from Figure 3 of Mallen et al.[13] due to overlap of data points, so only data for refractive error greater than 1.00 were digitized in order to extend the range of data beyond that of Atchison et al.[12] Ordinary least squares linear regression was used to determine the relationship and 95% prediction interval for the combined data. The 95% prediction interval was then used to simulate the error in estimating axial length from refractive error for input to the structure–function model (see Structure–Function Mapping Simulations section).

Structure–Function Mapping Simulations

The computational model used to generate structure–function maps was as previously described.[8] Briefly, the model maps a given set of visual field locations to the ONH in 1° sectors. In this study we use the 24-2 visual field locations ($n = 52$) as these are commonly used in clinical practice. The model's output depends on input biometric information (axial length, ONH position), and so is customized to the ocular anatomy of the individual patient. The model can be further customized (e.g., ONH dimensions, predisease neuroretinal rim dimensions), but in this study we only vary axial length and ONH position as these have the greatest effect on output maps (vertical ONH position mean $R^2 = 0.52$, horizontal ONH position mean $R^2 = 0.20$, and axial length mean $R^2 = 0.15$ from previous study).[8]

To assess the effect of measurement error in axial length and ONH position, a variety of clinically plausible inputs to the model were generated. The values were chosen to approximate the ranges of previously published clinical data[12–14] for patients with low to moderate refractive error. This was done under two conditions: where axial length was known, and where refractive error was known (but axial length was not). These parameters were considered the "true" values that were then to be measured clinically, inducing measurement error (see later). The Table shows the true anatomical parameters used in the simulations under each condition, every possible combination of these parameters was considered a simulated "patient."

For each combination of parameters in each condition ($n = 84$ for axial length known, $n = 126$ for refractive error known), we generated a set of 200 parameters with added measurement error according to the results of the investigations described in the ONH Position and Estimation of Axial Length from Refractive Error sections. Measurement error for fovea–ONH distance and angle was added by sampling from a Gaussian distribution with mean 0 and SD equal to the SD of within-

TABLE. The Parameters Used as Input to the Model Before Measurement Error Was Added

Parameter	Axial Length Known	Refractive Error Known
Axial length, mm	23, 24, 25, 26	-
Refractive error, D	-	−6.00, −4.00, −2.00, 0.00, +2.00, +4.00
Fovea–ONH distance, mm	4.0, 4.5, 5.0	4.0, 4.5, 5.0
Fovea–ONH angle, deg	−15, −12, −9, −6, −3, 0, 3	−15, −12, −9, −6, −3, 0, 3
Total combinations	84	126

The two conditions simulated are shown in separate columns, with the total number of simulated "patients" shown at the bottom of each column.

subject differences from the mean measurement (see Results section). In the refractive error known condition, axial length was estimated using the linear model fit, and measurement error added by sampling from a Gaussian distribution with mean 0 and central 95% equal to the width of the 95% prediction interval of the fitted model at the relevant refractive error (see Results section). In the axial length known condition we assume that the measurement error in biometry is negligible for our purposes, and therefore do not add measurement error to axial length. In this way, a total of 42,000 structure–function maps were generated, representing 200 repeated measurements of each of 210 simulated patients (84 with axial length known, 126 with refractive error known).

Different true anatomical parameters input to the model result in different mapped ONH sectors for each visual field location. To create a comparable metric for the effect of measurement error across all locations, the 1°-ONH sectors mapped from each visual field location for each simulated patient ($n = 200$ parameter sets) were normalized to represent angular difference from their mean. Normalized data were then combined across all simulated patients such that we report the 90% range widths (angular difference between the fifth and 95th percentile of the mapped 1° sectors) for each visual field location.

Clinical Case Examples

We present two glaucoma case examples to illustrate the use of custom structure–function mapping in clinical practice. The participants featured in the case examples gave written informed consent to participate and ethics approval was given by the University of Melbourne Human Research ethics committee. Data were collected according to the tenets of the Declaration of Helsinki. The data presented in the case examples are from four averaged OCT RNFL scans (Spectralis; Heidelberg Engineering GmbH) and a custom, high-spatial resolution (3° × 3° grid) visual field test (Octopus 900 perimeter; Haag-Streit AG, Koeniz, Switzerland, controlled via the Open Perimetry Interface[15]).

RESULTS

ONH Position

All captured OCT images were high quality (median image quality 33 dB, range, 25–41 dB). Figure 1 shows the variation in fovea–ONH angle and distance for each subject across 10 repeats. Within-subject variation in both measurements did not vary systematically with the mean (Spearman's $\rho = -0.31$, $P = 0.39$ for rank correlation between angle and variance of angle, Spearman's $\rho = 0.26$, $P = 0.47$ for rank correlation between distance and variance of distance) and was normally distributed around the mean measurement (confirmed by histograms and normal quantile–quantile plots). It was therefore considered appropriate to summarize the measurement error in fovea–ONH by their SDs from the mean. Standard deviation of repeat fovea–ONH angle measurements was 0.97°, and SD of repeat fovea–ONH distance measurements was 61 μm. These values were used as the SD of the Gaussian measurement error (mean = 0) added to the fovea–ONH angle and distance parameters in the simulations. For comparison, between-subject SD of mean fovea–ONH angle

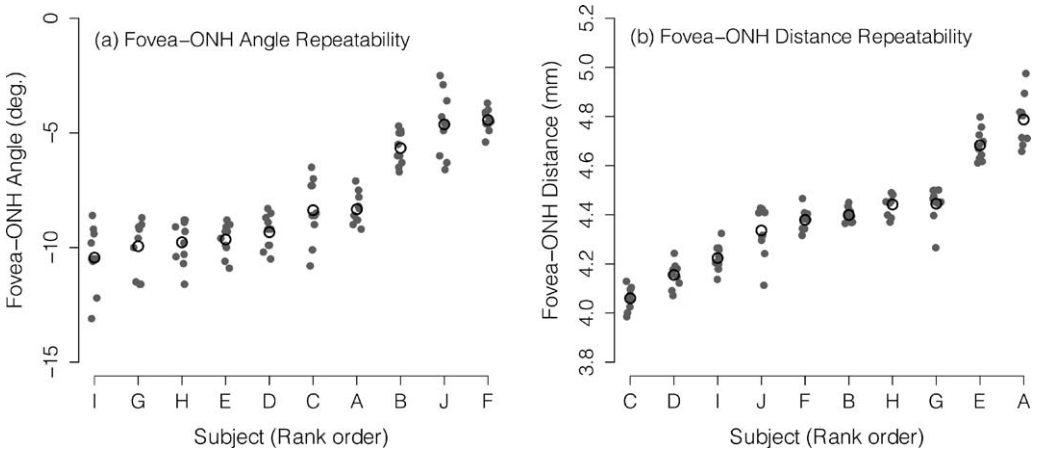

FIGURE 1. Repeatability of fovea-ONH angle (**a**) and distance (**b**) as measured using the optical coherence tomographer. Subjects are arranged along the horizontal axis in rank order for both plots. *Filled gray circles* show the 10 individual repeat measurements made on each subject, *unfilled black circles* show the mean of the 10 repeats.

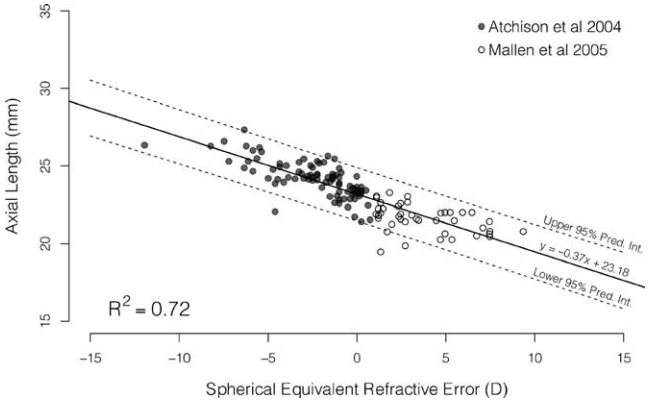

FIGURE 2. The relationship between spherical equivalent refractive error and axial length. Data were taken from two previous studies; *filled symbols* represent data from Atchison,[12] *unfilled symbols* represent data from Mallen.[13] The *solid line* represents the best fitting linear model by ordinary least squares linear regression (see text); *dashed lines* represent the 95% prediction interval of the model.

was 2.29°, and between-subject SD of mean fovea–ONH distance was 222 μm, indicating that for both measures between-subject variation was more than double within-subject variation in our sample.

Estimation of Axial Length From Refractive Error

Figure 2 shows the spherical equivalent refractive error versus axial length data taken from both previous studies.[12,13] The accuracy of the digitization process was confirmed by ordinary least squares linear regression on the data from Atchison et al.,[12] which yielded identical model coefficients, 95% confidence intervals (CIs), and R^2 to those reported in the original study. Figure 2 shows the best fitting linear model (ordinary least squares linear regression, $R^2 = 0.72$) to the combined data from both studies, and the 95% prediction interval for this model. The model had slope –0.37 mm/D (95% CI –0.41 to –0.33 mm/D) and intercept 23.18 mm (95% CI 23.03–23.33 mm). The width of the 95% prediction interval at the appropriate refractive error was used as the central 95% of the Gaussian measurement error (mean = 0) added to the model prediction of axial length in the simulations.

Structure–Function Mapping Simulations

For each of the parameter combinations shown in the Table ($n = 84$ for the axial length known condition, $n = 126$ for the refractive error known condition), 200 structure function maps were generated with added measurement error. Therefore, we generated 16,800 different maps for the axial length known condition, and 25,200 different maps for the refractive error known condition.

Figure 3 shows all the 1°-ONH sectors mapped from each visual field location under each condition for the input anatomical parameters simulated. Note that some locations in the nasal step area can map to either side of the ONH depending on anatomy, as described previously.[8] In brief, this situation occurs when the ONH position is such that a line extended through the ONH and the fovea passes the visual field point on the opposite side to that conventionally expected, making the opposite side of the ONH closer to the visual field point.

Figure 4 shows the 90% range widths of normalized mapped sectors across all simulated patients repeated with measurement errors. Circle sizes at each location are proportional to the variation in mapping (also given numerically). Data are shown at each visual field location, under each measurement error condition. At some locations in the nasal step area a second circle represents the 90% range width of the minor component of the bimodal distribution where locations can map to either side of the ONH depending on anatomical parameters.[8] For simulated patients who did not produce bimodal distributions of mapped angles at these locations,

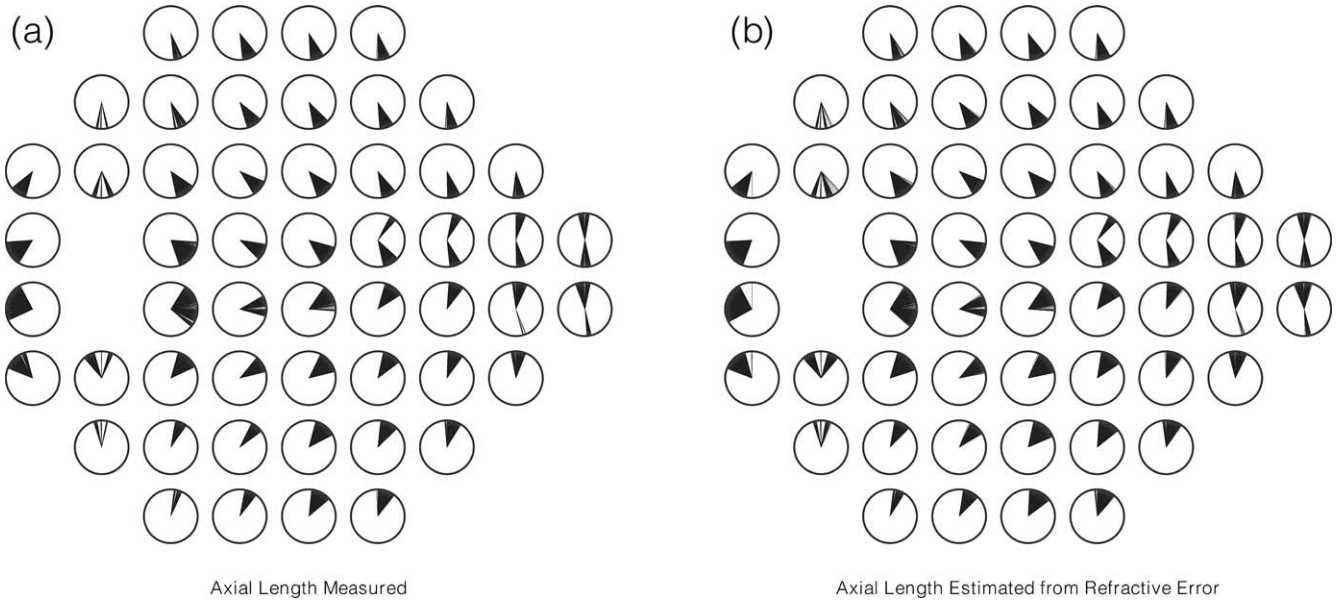

FIGURE 3. The 1° ONH sectors mapped from each 24-2 visual field location when axial length input to the model is (**a**) measured accurately and (**b**) estimated from refractive error. *Shaded areas* represent the mapped sectors. Note that, in general, locations in the superior visual field map to the inferior ONH and vice versa due to the inversion of the visual field relative to the retina.

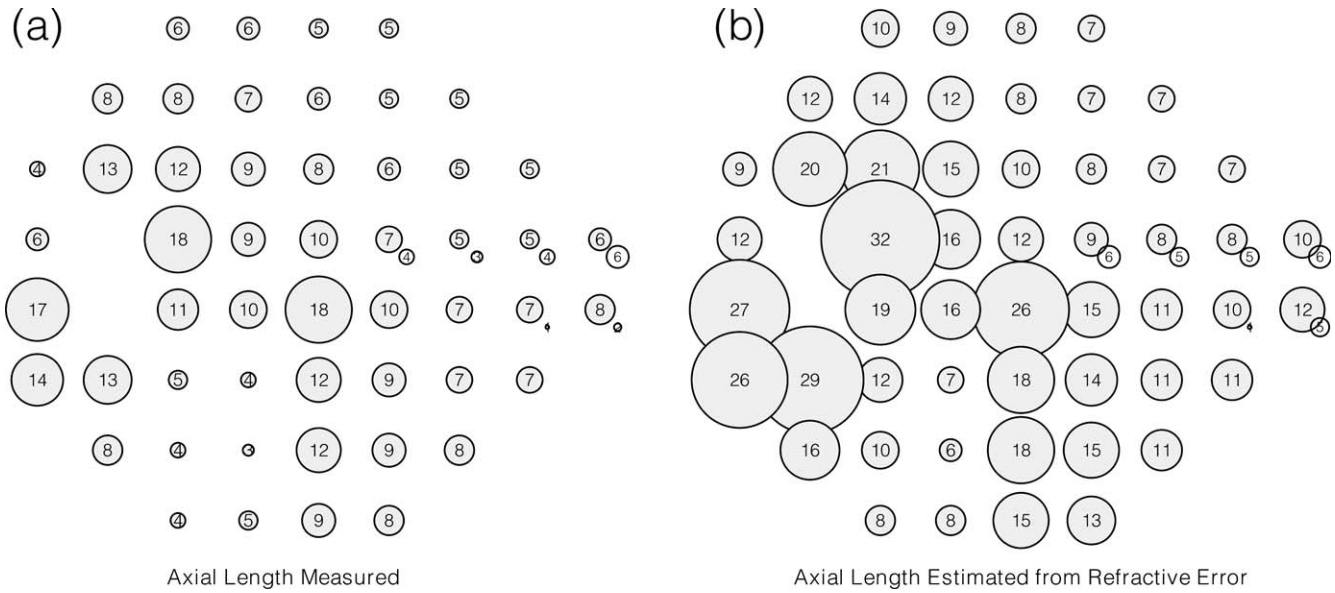

FIGURE 4. Ninety percent range widths of normalized mapped sectors across all simulated patients repeated with measurement error only in ONH position (**a**) and with measurement error in optic nerve head position and error in estimating axial length from refractive error (**b**). Circle size at each location is proportional to the variation in mapping, which is also given numerically. Six locations in the nasal step area exhibited bimodal variation in mapping, mapping to opposite sides of the horizontal midline according to anatomy. Second *unshaded circles* at these locations show the 90% range width of the minor distribution (the distribution of sectors mapped on the less frequently mapped side of the ONH).

angles were treated the same as the major component of bimodal distributions produced. Ninety percent range widths varied from 3° to 18° when axial length was measured accurately, and from 6° to 32° when axial length was estimated from refractive error. Comparison of individual locations showed that 90% range widths were median 4° (interquartile range, 3°–6°) bigger when axial length was estimated than when it was measured. The 90% range widths can be considered to represent the precision of custom structure–function mapping when clinical data are used as input to the model. For research use, sector sizes could be customized to each location using these ranges, or could be continuous, using a moving window of appropriate fixed or variable size. For routine clinical use, however, it is probably more appropriate to use a single, fixed size for ONH sectors in order to facilitate easy interpretation by a range of clinicians.

Figures 5 and 6 show examples of how custom structure–function mapping might be applied clinically to visual field and OCT data from patients with glaucoma. Data are shown from detailed visual field examination (Figs. 5a, 6a) and the average of four RNFL circle scans from OCT (Figs. 5c, 6c). Based on the ranges shown in Figure 4 we used 30° ONH sectors for structure–function mapping, which is wide enough to capture all of the 90% ranges when axial length is measured accurately, or all but one (32°) when axial length is estimated from refractive error (Fig. 4). For the fixed sectors that we recommend for general clinical use, the first sector is centered on the fovea–ONH axis, and the others adjoin around the ONH. A color-coded map using this scheme, customized to the anatomical data of the patient is shown in Figures 5b and 6b. Figures 5d, 5e, 6d, and 6e show combined structure–function plots to aid visualization of concordance between the two measures. Figures 5d and 6d use continuous ONH sectors, such that the sector used for each visual field location is a 30° sector centered on the angle predicted by the model (this means that sectors can overlap, and areas of the ONH may not be mapped to at all since the visual field locations do not cover the entire retina). Figures 5e and 6e use the simpler fixed 30° sectors as shown in Figures 5b, 5c, 6b, and 6c.

Figure 5a shows a deep, localized inferior paracentral visual field defect, as well as more mild defects affecting the area superior to the physiological blind spot and the nasal step area. The paracentral scotoma appears concordant with the area of apparent RNFL thinning at approximately 20° to 50°, while the milder defects superior to the blind spot and in the nasal step area may be consistent with another area of apparent thinning around 260° to 280° (Figs. 5c–e).

Data from a patient with advanced glaucoma are shown in Figure 6. Almost all locations in the visual field plot (Fig. 6a) are perimetrically blind, except for remaining areas of vision centrally and temporal to the blind spot. Circumpapillary RNFL thickness is also well below population norms in many areas, with only a few regions remaining within normal limits. As can be seen in Figures 6c through 6e, the areas of remaining vision correspond well with the nasal and temporal areas of thicker RNFL, while the regions of deep visual field loss are generally predictable from the regions of apparent RNFL thinning.

DISCUSSION

Structure–function maps currently in widespread clinical use represent population average relationships and may not accurately describe individual patients. Our data, and that of others, demonstrate considerable variation in the ocular anatomical parameters that affect individual relationships between regions of the ONH and the visual field.[5,6,8,9] Consequently, it may be clinically advantageous to customize structure–function maps to the anatomy of the individual patient when considering structural imaging data and visual field data together.

Our previously described model[7,8] produces structure–function maps customized to the input anatomical parameters relating to the individual patient. Maps can be produced

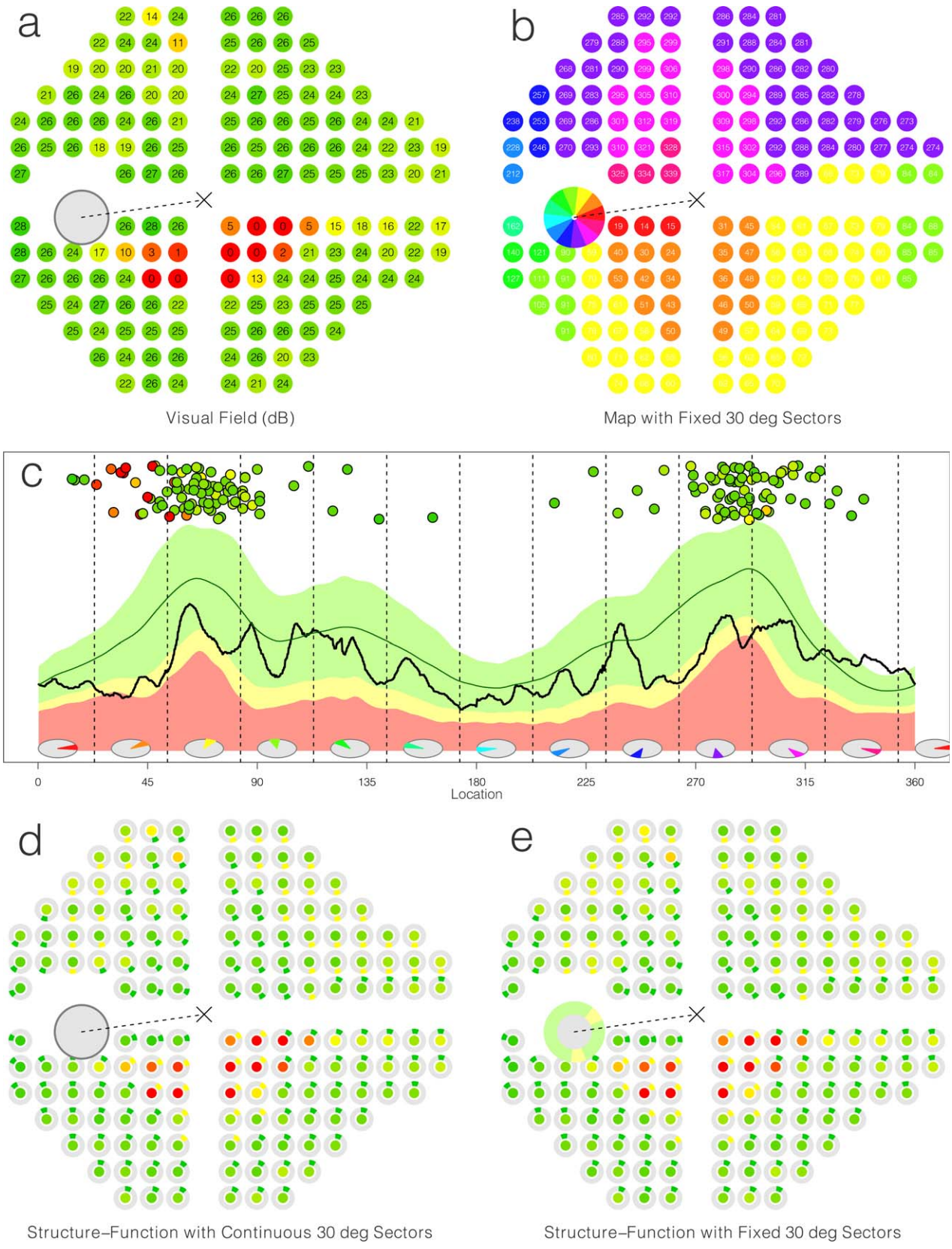

Figure 5. Clinical example of a 64-year-old female with glaucoma. The patient had an axial length of 22.89 mm, a fovea-ONH distance of 4.03 mm, and a fovea-ONH angle of −8.13°. (**a**) Visual field plot with dense stimulus pattern (3° × 3° grid), *red points* represent areas of poor sensitivity. Optic nerve head position and fovea–ONH axis are indicated. (**b**) Custom structure–function map with color-coded 30° sectors. The *red sector* is centered on the indicated fovea–ONH axis, remaining sectors adjoin around the ONH. The number at each location represents the 1° ONH sector mapped to. (**c**) Retinal nerve fiber layer thickness (*black line*) as measured by OCT. The 30° ONH sectors shown in (**b**) are designated by the *vertical dashed lines* and the schematics in each sector. Visual field points, color-coded as in (**a**) are shown along the *top*, positioned horizontally according to their

Investigative Ophthalmology & Visual Science

mapped 1° ONH sector. (**d**) Structure–function map using continuous 30° sectors. At each visual field location the visual field sensitivity (*central filled circle*) is color-coded as in (**a**), and the surrounding *gray ring* contains a 30° sector color-coded according to the RNFL thickness relative to population norms (**c**). The continuous sectors are centered on the 1° sector shown in (**b**) so may overlap and may not cover the entire ONH circumference. (**e**) Structure–function map as in (**d**) but using the fixed 30° sectors as shown in (**b**) and as represented by the *dotted lines* and schematic diagrams in (**c**). The circumference of the ONH is shaded according to the RNFL thickness relative to population norms as shown in (**c**).

relating any visual field pattern to the ONH for use with any imaging methodology; however, the precision with which the input anatomic parameters are measured is a limiting factor in the precision and, therefore, minimum ONH sector size of the output map. In this study, we have considered the effects on output maps of variability in measurements of ONH position using a clinically available technique, and of the errors inherent in estimating axial length from refractive error. The pattern of variability in output maps across the visual field (Figs. 3, 4) is consistent with the effects of axial length and ONH position shown in both our own previous study[8] and a recent empirical study.[6]

Based on the variability in output maps resulting from measurement errors in input parameters we have demonstrated the minimum ONH sector sizes that are feasible for use at each of the 24-2 visual field locations under conditions where axial length is accurately measured, and also where axial length can only be estimated from refractive error (Fig. 4). For general clinical use, we suggest a simple scheme of 30° ONH sectors with the first sector centered on the fovea–ONH axis and the remaining sectors adjoining around the ONH, though note that under this scheme there will still be variations in the number and location of visual field points mapping to the ONH sectors. While accurately measuring axial length yields smaller minimum feasible ONH sector sizes, we have also demonstrated, based on previously published data,[12,13] that for clinical purposes estimating the axial length input parameter from refractive error is sufficiently accurate and precise for the use of 30° sectors, and indeed has little impact in some areas of the visual field (Fig. 4). The use of smaller or continuous ONH sectors may be appropriate in some circumstances, particularly in a research environment where increased resolution in mapping may be desired; however, it should be remembered that larger sectors hold advantages such as being less vulnerable to the effects of small inaccuracies in mapping and of imperfections in the imaging and visual field measurements. A further consideration that impacts choice of sector-size for users of any structure–function mapping scheme is how to summarize data within sectors. A detailed discussion of possible summary statistics is outside the scope of this article, but it is worth mentioning that averaging data within larger sectors holds potential to mask small, localized defects, and so these trade-offs require careful consideration by users depending on their own purpose.

The ranges of variability found in this study are not without caveats. For some patients, measurement errors in ONH position or estimation errors in axial length may be larger than those found here. The 10 subjects of our ONH position experiment were all young, healthy observers with normal posture and mobility, and the published data used for estimating axial length from refractive error also relates to observers without eye disease or history of eye surgery. Postural problems may render the measured ONH position inaccurate unless adequately compensated for, while the presence of cataract or history of cataract or refractive surgery may render estimation of axial length from refractive error inaccurate. It should be noted that these caveats apply not only to our custom structure–function model, but also to any other mapping scheme, including the population maps currently in widespread use.

Many studies have investigated the relationship between structural and functional changes in glaucoma.[16,17] From these studies it is clear that although measurements from ONH or RNFL imaging and perimetry are related, the relationship is far from perfect. In addition to measurement error and variability,[18] many reasons exist for discordance between structural and functional measures in individual patients, for example, the effects on imaging measurements of blood vessels and glial tissue, and the effects on perimetric measurements of spatial stimulus localization, retinal and higher visual processing, and attention. Because the structure–function relationship is imperfect, it is unrealistic to expect perfect spatial correspondence between measured defects in ONH or RNFL parameters and the visual field. Nevertheless, it seems likely that customizing structure–function maps to individual anatomy will improve this spatial correspondence in many patients, and therefore represent a step forward in the clinical appraisal of glaucomatous damage.

An assumption of our model is that the spatial relationship between retinal locations and the ONH or RNFL is entirely defined by the retinal ganglion cell axons that connect them. This is also an assumption of most other structure–function mapping schemes, however, it is known that in the central 3° of the human macula retinal ganglion cells are laterally displaced from their corresponding photoreceptors by up to approximately 2° of visual angle.[19–21] This displacement may represent a source of error in this area when using the model for centrally dense visual field patterns such as the 10-2 pattern. Future iterations of our model may incorporate these details in order to produce individualized maps of the macula area for use with such visual field patterns. The most central locations of the 24-2 pattern commonly used clinically are 4.24° from fixation, and so are relatively unaffected by this displacement.

In this paper, we have presented two case examples of glaucoma patients whose visual fields have been measured with a spatially dense perimetric grid pattern. These cases are presented herein to demonstrate how custom structure–function mapping might be applied to clinical data, and to demonstrate the 30° ONH sectors suggested. Of course, a much larger study is needed to investigate the spatial concordance between structural and functional defects in glaucoma, and ideally such a study would consider disease progression in both domains, rather than departures from population norms. It would then be possible to gauge the clinical benefit of using customized structure–function maps over existing population average maps.

In conclusion, we have demonstrated that it is feasible to apply custom structure–function mapping to the clinical management of patients with glaucoma or other optic neuropathies. The anatomical parameters that are most important to the model, ONH position and axial length, can be estimated from readily available clinical information with sufficient accuracy and precision for this purpose. The minimum feasible ONH sector size for custom structure–function mapping using our model varies across the visual

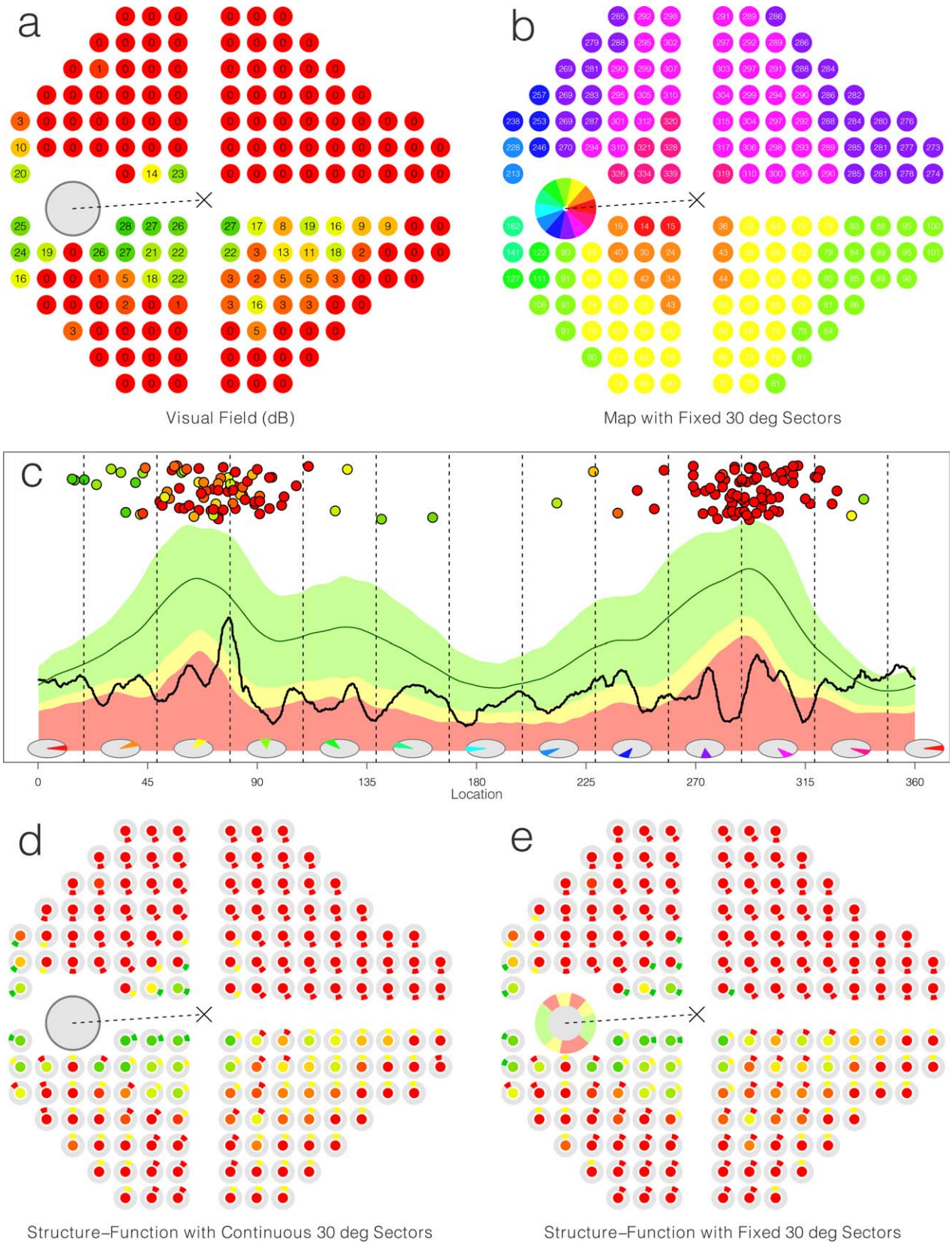

FIGURE 6. Clinical example of a 76-year-old male with advanced glaucoma. The patient had an axial length of 23.85 mm, a fovea-ONH distance of 4.37 mm, and a fovea-ONH angle of −3.81°. Panels are as described for Figure 5.

field, but for general clinical use a simple scheme of 30° sectors is suggested.

Acknowledgments

The authors thank Shonraj Ballae Ganeshrao for collecting the data presented in the two case examples. Heidelberg Engineering GmbH provided the normative data shown in the OCT profiles in Figures 5 and 6.

Supported by a Victorian Life Sciences Computation Initiative (VLSCI) Grant VR0052 on its Peak Computing Facility at the University of Melbourne, an initiative of the Victorian Government, Australia, the Australian Research Council (ARC) Linkage Project LP100100250 (with Heidelberg Engineering, GmbH), two ARC Future Fellowships FT0990930 (AMM), and FT0991326 (AT).

Disclosure: **J. Denniss**, Heidelberg Engineering GmbH (F); **A. Turpin**, Heidelberg Engineering GmbH (F), Haag-Streit AG (F); **A.M. McKendrick**, Heidelberg Engineering GmbH (F), Haag-Streit AG (F)

References

1. Garway-Heath DF, Holder GE, Fitzke FW, Hitchings RA. Relationship between electrophysiological, psychophysical, and anatomical measurements in glaucoma. *Invest Ophthalmol Vis Sci*. 2002;43:2213–2220.
2. Garway-Heath DF, Poinoosawmy D, Fitzke FW, Hitchings RA. Mapping the visual field to the optic disc in normal tension glaucoma eyes. *Ophthalmology*. 2000;107:1809–1815.
3. Jansonius NM, Nevalainen J, Selig B, et al. A mathematical description of nerve fiber bundle trajectories and their variability in the human retina. *Vision Res*. 2009;49:2157–2163.
4. Ferreras A, Pablo LE, Garway-Heath DF, Fogagnolo P, Garcia-Feijoo J. Mapping standard automated perimetry to the peripapillary retinal nerve fiber layer in glaucoma. *Invest Ophthalmol Vis Sci*. 2008;49:3018–3025.
5. Jansonius NM, Schiefer J, Nevalainen J, Paetzold J, Schiefer U. A mathematical model for describing the retinal nerve fiber bundle trajectories in the human eye: average course, variability, and influence of refraction, optic disc size and optic disc position. *Exp Eye Res*. 2012;105:70–78.
6. Lamparter J, Russell RA, Zhu H, et al. The influence of inter-subject variability in ocular anatomical variables on the mapping of retinal locations to the retinal nerve fiber layer and optic nerve head. *Invest Ophthalmol Vis Sci*. 2013;54:6074–6082.
7. Turpin A, Sampson GP, McKendrick AM. Combining ganglion cell topology and data of patients with glaucoma to determine a structure-function map. *Invest Ophthalmol Vis Sci*. 2009;50:3249–3256.
8. Denniss J, McKendrick AM, Turpin A. An anatomically customizable computational model relating the visual field to the optic nerve head in individual eyes. *Invest Ophthalmol Vis Sci*. 2012;53:6981–6990.
9. Denniss J, Turpin A, Tanabe F, Matsumoto C, McKendrick AM. Structure-function mapping: variability and conviction in tracing retinal nerve fiber bundles and comparison to a computational model. *Invest Ophthalmol Vis Sci*. 2014;55:728–736.
10. Stenstrom S. Investigation of the variation and the covariation of the optical elements of human eyes. *Am J Optom Arch Am Acad Optom*. 1948;25:388–397.
11. Benjamin B, Davey JB, Sheridan M, Sorsby A, Tanner JM. Emmetropia and its aberrations; a study in the correlation of the optical components of the eye. *Spec Rep Ser Med Res Counc (G B)*. 1957;11:1–69.
12. Atchison DA, Jones CE, Schmid KL, et al. Eye shape in emmetropia and myopia. *Invest Ophthalmol Vis Sci*. 2004;45:3380–3386.
13. Mallen EAH, Gammoh Y, Al-Bdour M, Sayegh FN. Refractive error and ocular biometry in Jordanian adults. *Ophthalmic Physiol Opt*. 2005;25:302–309.
14. Chauhan BC, Burgoyne CF. From clinical examination of the optic disc to clinical assessment of the optic nerve head: a paradigm change. *Am J Ophthalmol*. 2013;156:218–227.
15. Turpin A, Artes PH, McKendrick AM. The open perimetry interface: an enabling tool for clinical visual psychophysics. *J Vision*. 2012;12:22.
16. Harwerth RS, Wheat JL, Fredette MJ, Anderson DR. Linking structure and function in glaucoma. *Prog Retin Eye Res*. 2010;29:249–271.
17. Malik R, Swanson WH, Garway-Heath DF. 'Structure-function relationship' in glaucoma: past thinking and current concepts. *Clin Experiment Ophthalmol*. 2012;40:369–380.
18. Hood DC, Anderson SC, Wall M, Raza AS, Kardon RH. A test of a linear model of glaucomatous structure-function loss reveals sources of variability in retinal nerve fiber and visual field measurements. *Invest Ophthalmol Vis Sci*. 2009;50:4254–4266.
19. Drasdo N, Leigh Millican C, Katholi CR, Curcio CA. The length of Henle fibers in the human retina and a model of ganglion receptive field density in the visual field. *Vision Res*. 2007;47:2901–2911.
20. Curcio CA, Allen KA. Topography of ganglion cells in human retina. *J Comp Neurol*. 1990;300:5–25.
21. Hood DC, Raza AS, de Moraes CG, Liebmann JM, Ritch R. Glaucomatous damage of the macula. *Prog Retin Eye Res*. 2013;32:1–21.

Investigative Ophthalmology & Visual Science